Available online at www.sciencedirect.com
ScienceDirect
European Journal of Medicinal Chemistry 43 (2008) 142–154
EUROPEAN JOURNAL OF MEDICINAL CHEMISTRY
http://www.elsevier.com/locate/ejmech

Original article

Insights into the structural requirements of farnesyltransferase inhibitors as potential anti-tumor agents based on 3D-QSAR CoMFA and CoMSIA models

Devendra S. Puntambekar, Rajani Giridhar, Mange Ram Yadav*

Pharmacy Department, Faculty of Technology and Engineering, The M.S. University of Baroda, Kalabhavan, PO Box 51, Baroda 390 001, Gujarat, India

Received 1 December 2006; received in revised form 5 January 2007; accepted 1 February 2007
Available online 25 February 2007

Abstract

A three-dimensional quantitative structure–activity relationship (3D-QSAR) study was performed on three different chemical series reported as selective farnesyltransferase (FTase) inhibitors employing comparative molecular field analysis (CoMFA) and comparative molecular similarity indices (CoMSIA) techniques to investigate the structural requirements for substrates and derive a predictive model that may be used for the design of novel FTase inhibitors. Removal of outliers improved the predictive power of models developed for all three structurally diverse classes of compounds. 3D-QSAR models were derived for 3-aminopyrrolidinone derivatives (training set $N = 38$, test set $N = 7$), 2-amino-nicotinonitriles (training set $N = 46$, test set $N = 13$) and 1-aryl-1′-imidazolyl methyl ethers (training set $N = 35$, test set $N = 5$). The CoMFA models with steric and electrostatic fields exhibited r^2_{cv} 0.479–0.803, r^2_{ncv} 0.945–0.993, r^2_{pred} 0.686–0.811. The CoMSIA models displayed r^2_{cv} 0.411–0.814, r^2_{ncv} 0.923–0.984, r^2_{pred} 0.399–0.787. 3D contour maps generated from these models were analyzed individually, which provide the regions in space where interactive fields may influence the activity. The superimposition of contour maps on the active site of farnesyltransferase additionally helps in understanding the structural requirements of these inhibitors. 3D-QSAR models developed may guide our efforts in designing and predicting the FTase inhibitory activity of novel molecules.

Keywords: CoMFA; CoMSIA; Farnesyltransferase inhibitors; Anticancer; 3-Aminopyrrolidinones; 2-Amino-nicotinonitriles; 1-Aryl-1′-imidazolyl methyl ethers

1. Introduction

The need for new chemotherapeutics in cancer is evident from the limited capacity of existing drugs to cure or significantly prolong the survival of patients with disseminated tumors or certain leukemias. The explosion of information on the biological complexities of cancer and the molecular genetic defects underlying tumorigenesis has afforded new opportunities for anticancer drug discovery and development [1,2]. Mutation of the GTP-binding protein Ras, a central player in cell signaling pathways that govern cell growth, can lead to cellular transformation and uncontrolled proliferation [3]. The observation that mutant Ras genes are often found in human tumors suggests that inhibition of Ras function might provide an effective anticancer therapy [4,5]. Extensive studies on Ras have revealed that a series of posttranslational modifications are required for its biological function, the first step of which is alkylation of a cysteine residue near its C-terminus with a farnesyl group [6,7]. Thus, the enzyme farnesyltransferase (FTase), which catalyses this step, was identified as a potential target for chemotherapeutic agents. FTase is a zinc heterodimeric metalloenzyme consisting of two subunits: the first weighs 48 kDa (α) [8] and the latter 46 kDa (β) [9]. The zinc ion is placed at a junction between a hydrophilic surface of the α subunit and a deep cleft in the β subunit lined by aromatic residues. The zinc is coordinated by Asp297β, Cys299β, His362β residues and a water molecule.

* Corresponding author. Tel.: +91 265 2434187; fax: +91 265 2418927.
E-mail address: mryadav11@yahoo.co.in (M.R. Yadav).

0223-5234/$ - see front matter © 2007 Elsevier Masson SAS. All rights reserved.
doi:10.1016/j.ejmech.2007.02.003

The FTase substrates can be investigated as models for designing selective FTase inhibitors [10] and thus all novel inhibitors can be classified as (a) molecules designed on the Ca_1a_2X motif (peptidomimetics), which interact with the same FTase residues involved in the Ras binding proteins [11], (b) molecules designed on the farnesyl moiety (FPP mimetics), which interact with the FPP binding site [12], and (c) bisubstrate inhibitors, which incorporate structural motifs of both FPP and Ca_1a_2X tetrapeptide [13–16].

Most inhibitors described in the literature are peptidomimetics resembling the CAAX-tetrapeptide recognition sequence of farnesylated proteins. Majority of these CAAX-peptidomimetics exhibit a free thiol group [13–16,17] which is believed to coordinate the enzyme-bound zinc ion as shown for the native peptide substrate [18]. However, free thiols are associated with several adverse drug effects [19] and thus the development of farnesyltransferase inhibitors is clearly directed towards the so-called non-thiol farnesyltransferase inhibitors. Most frequently used replacements for cysteine are nitrogen-containing heterocycles. The ring nitrogen is supposed to coordinate to the enzyme-bound zinc similar to the cysteine thiol group [20]. However, it has been showed that nitrogen heterocycles can be replaced by aryl residues lacking the ability to coordinate metal atoms without losing too much of their farnesyltransferase inhibitory activity [21,22]. Therefore, the existence of at least one hitherto unknown aryl-binding region in the farnesyltransferase active site has been postulated [23,24]. Several farnesyltransferase inhibitors (FTIs) have been developed by academic and industry researchers and have been tested extensively in preclinical in vitro and in vivo cancer models [25–36]. Some of these inhibitors exhibiting binding constants in the nanomolar range are still being developed as drug candidates. No significant breakthrough has occurred in achieving the essential requirements for a therapeutic agent in the treatment of cancer based on FTase inhibition.

The 3D-QSAR, CoMFA method was proposed by Crammer et al. in 1988, which is extensively used in the present practice of drug discovery [37]. One of the advantages of CoMFA is the ability to predict the biological activity of the molecules by deriving a relation between steric/electrostatic properties and biological activities in the form of contour maps. CoMFA calculates steric fields using Leonard–Jones potential and electrostatic fields using Coulombic potential. In particular, both of the potential functions are very steep near the van der Waals surface of the molecule, causing rapid changes in the surface descriptions and requiring the use of cutoff values so that calculations are not done within the molecular surface. In addition, a scalar factor is applied to the steric field, so that both fields can be used in the same PLS (partial least-squares) analysis. Finally, changes in the orientation of the superimposed molecular set, relative to the calculation grid, can cause significant change in the CoMFA results, again probably due to strict cutoff values. The alignment rule is one of the most sensitive input areas for CoMFA studies. Several improvements have been made in the alignment methodology: addition of macroscopic descriptor(s) in the study table and a reverse method of CoMFA, called AFMoC (adaptation of fields for molecular comparison) and topomer CoMFA have been introduced [38–41]. The CoMSIA method of 3D-QSAR analysis was introduced by Klebe et al. [42] in 1994, in which using a common probe atom, similarity indices are calculated at regularly placed grid points for the prealigned molecules. CoMSIA is not sensitive to changes in the orientation of the superimposed molecules in the lattice, and the correlation results obtained by CoMSIA can be graphically interpreted in terms of the field contribution maps allowing physicochemical properties relevant for binding to be easily mapped back on to molecular structures [43,44].

Previously, we have reported 3D-QSAR models for a series of benzonitrile and tricyclicpiperazinyl derivatives [45,46] as farnesyltransferase inhibitors. The present study is aimed at elucidating the structural features required for FTase inhibition and to obtain predictive three-dimensional quantitative structure activity relationship (3D-QSAR) models, which may guide the rational synthesis of novel compounds (Fig. 1). In the present paper, we report the 3D-QSAR models derived from the most widely used computational tools: comparative molecular field analysis (CoMFA)/comparative molecular similarity indices (CoMSIA) methods, for structurally diverse sets of FTase inhibitors from the literature.

2. Results and discussion

The 3D-QSAR models derived using CoMFA and CoMSIA methodologies were characterized by different chemical

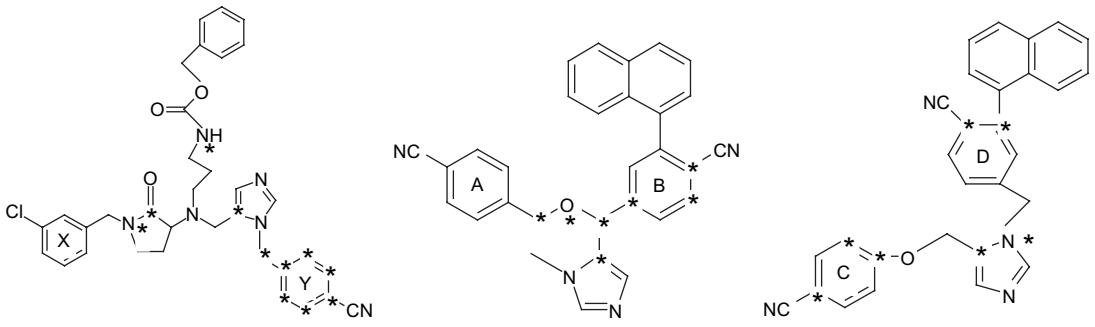

47 97 152

Fig. 1. Template structures and (hetero) atoms used in the rms alignment.

classes published in the literature [11–13]. The structures and biological activity data of the molecules are described in Tables S1–S3 (see Supporting information). The in vitro FTase inhibitory activity values pIC_{50} (nM) was used as dependent variable and CoMFA/CoMSIA fields as independent variables in the study. The low energy conformer obtained from Multi-Search option in Sybyl was used in the molecular alignment method performed by atom-based rms fitting. As CoMFA is alignment sensitive, different alignment rules were employed but only the alignment yielding best results have been discussed. One of the major obstacles in the 3D-QSAR studies lies with the 'congeners', which misfit the final equation and were termed as outliers. The reasons for the poor prediction may be their structural uniqueness or the insignificant mathematical value in defining the biological activity. Exceptions are also observed wherein experimentally observed parameters might be better than the calculated or vice versa: however, their inclusion in 3D-QSAR studies at the cost of lower r^2 could be more confusing than being helpful.

The 3D-QSAR models were generated from training set molecules and validated by predicting activity of test set molecules. All cross-validated results were analyzed by considering the fact that the value of r^2_{cv} above 0.3 indicates that the probability of chance correlation is less than 5%. The results of PLS analysis are summarized from CoMFA studies in Table 1 and that from CoMSIA studies in Tables 2–4. Comparison of the statistical results of the best models obtained by CoMFA and CoMSIA are summarized in Table 5.

2.1. CoMFA models

2.1.1. 3-Aminopyrrolidinone derivatives

3D-QSAR models for 3-aminopyrrolidinones reported by Bell et al. [47] as selective FTase inhibitors (Table S1) were initially developed using 41 training set molecules and validated by predicting activity for nine test set molecules (Analysis A). The CoMFA model developed from steric and electrostatic fields yielded cross-validated r^2 (r^2_{cv}) 0.526 at seventh component, non-cross-validated r^2 (r^2_{ncv}) 0.928, predictive r^2 (r^2_{pred}) 0.475 and higher contribution of electrostatic field (53.2%) than steric (46.8%) field. In order to improve the predictive power of the model, four compounds whose residual values were on higher side were considered as outliers and subsequent analysis (Analysis B) was carried out. The CoMFA model developed yielded cross-validated r^2 (r^2_{cv}) 0.596 at sixth component, non-cross-validated r^2 (r^2_{ncv}) 0.945 with lower standard error of estimate (0.224), predictive r^2 (r^2_{pred}) increased as high as 0.790. A high bootstrapped r^2 of 0.971 adds a high confidence limit to this analysis. In this analysis both steric and electrostatic fields contribute to the QSAR equation by 45.5% and 54.5%, respectively, suggesting that variation in biological activity of inhibitors is dominated by

Table 1
Summary of CoMFA results from atom-based rms alignment

	I[a]		II[b]		III[c]	
	Analysis A	Analysis B	Analysis A′	Analysis B′	Analysis A″	Analysis B″
r^2_{cv}	0.526	0.596	0.403	0.803	0.346	0.479
N_c	7	6	2	4	11	8
SEP	0.615	0.414	0.463	0.285	0.403	0.422
r^2_{ncv}	0.928	0.945	0.893	0.983	0.998	0.993
SEE	0.251	0.224	0.189	0.089	0.024	0.048
F-Value	44.587	62.660	180.441	261.653	1112.47	373.34
$P\ r^2 = 0$	0.0	0.0	0.0	0.0	0.0	0.0
Contribution (fraction)						
S	0.468	0.485	0.455	0.542	0.374	0.389
E	0.532	0.515	0.545	0.458	0.626	0.611
r^2_{pred}	0.475	0.790	0.357	0.811	0.289	0.686
r^2_{bs}	0.967	0.971	0.913	0.988	–	0.996
Std dev	0.014	0.013	0.089	0.004	–	0.003

[a] 3-Aminopyrrolidinone derivatives.
[b] 2-Amino-nicotinonitriles.
[c] 1-Aryl-1′-imidazolyl methyl ethers.

Table 2
Summary of CoMSIA results for 3-aminopyrrolidinone derivatives

	HAD	SEDAH	SDAH	SDH	SDA	SEA	SEDA	SEDH
r^2_{cv}	0.313	0.469	0.256	0.330	0.419	0.290	0.300	0.451
N_c	7	8	7	8	8	9	4	8
SEP	0.724	0.648	0.754	0.728	0.678	0.763	0.696	0.659
r^2_{ncv}	0.898	0.923	0.914	0.922	0.846	0.904	0.713	0.938
SEE	0.280	0.247	0.261	0.248	0.249	0.280	0.445	0.222
F-Value	36.331	41.883	37.188	41.343	19.218	28.268	19.913	52.750
$P\ r^2 = 0$	0.0	0.0	0.0	0.0	0.0	0.0	0.0	0.0
Contribution (fraction)								
S	–	0.122	0.151	0.559	0.270	0.233	0.161	0.154
E	–	0.211	–	–	–	0.376	0.301	0.294
H	0.461	0.306	0.381	0.219	–	–	–	0.401
D	0.186	0.127	0.157	0.222	0.232	–	0.112	0.151
A	0.353	0.234	0.311	–	0.498	0.390	0.426	–
r^2_{pred}	0.653	0.787	0.646	0.688	0.606	0.516	0.665	0.534
r^2_{bs}	0.925	0.962	0.952	0.967	0.897	0.955	0.843	0.960
Std dev	0.025	0.023	0.028	0.016	0.026	0.023	0.061	0.011

S = steric, E = electrostatic, D = H-bond donor, A = H-bond acceptor, and H = hydrophobic.

Table 3
Summary of CoMSIA results for 2-amino-nicotinonitriles

	HAD	SEDAH	SDAH	SDH	SDA	SEA	SEDA	SEDH
r^2_{cv}	0.747	0.814	0.705	0.628	0.651	0.718	0.806	0.827
N_c	10	5	5	4	4	4	4	5
SEP	0.350	0.280	0.353	0.392	0.380	0.341	0.283	0.271
r^2_{ncv}	0.958	0.931	0.868	0.790	0.754	0.927	0.874	0.939
SEE	0.143	0.171	0.236	0.294	0.318	0.174	0.228	0.102
F-Value	79.172	101.184	52.742	38.598	31.454	130.014	71.046	100.269
$P\ r^2 = 0$	0.0	0.0	0.0	0.0	0.0	0.0	0.0	0.0
Contribution (fraction)								
S	–	0.085	0.133	0.269	0.220	0.102	0.112	0.122
E	–	0.306	–	–	–	0.517	0.371	0.439
H	0.487	0.214	0.324	0.527	–	–	–	0.285
D	0.092	0.187	0.217	0.204	0.229	–	0.209	0.154
A	0.422	0.207	0.326	–	0.551	0.320	0.308	–
r^2_{pred}	0.724	0.784	0.757	0.570	0.627	0.634	0.747	0.695
r^2_{bs}	0.976	0.939	0.896	0.822	0.764	0.937	0.885	0.948
Std dev	0.010	0.019	0.032	0.031	0.037	0.016	0.027	0.014

S = steric, E = electrostatic, D = H-bond donor, A = H-bond acceptor, and H = hydrophobic.

Table 4
Summary of CoMSIA results for 1-aryl-1′-imidazolyl methyl ethers

	HAD	SEDAH	SDAH	SDH	SDA	SEA	SEDA	SEDH
r^2_{cv}	0.124	0.382	0.382	0.284	0.392	0.357	0.411	0.338
N_c	2	6	10	6	8	7	8	7
SEP	0.477	0.434	0.478	0.467	0.451	0.454	0.444	0.460
r^2_{ncv}	0.443	0.988	0.995	0.916	0.934	0.973	0.984	0.968
SEE	0.380	0.065	0.042	0.160	0.149	0.092	0.074	0.101
F-Value	10.73	181.10	388.45	41.99	36.903	114.93	158.62	95.033
$P\ r^2 = 0$	0.0	0.0	0.0	0.0	0.0	0.0	0.0	0.0
Contribution (fraction)								
S	–	0.183	0.108	0.378	0.321	0.168	0.093	0.189
E	–	0.513	–	–	–	0.458	0.266	0.488
H	0.328	0.299	0.190	0.619	–	–	–	0.319
D	0.069	0.005	0.003	0.003	0.002	–	0.008	0.008
A	0.602	0.190	0.221	–	0.677	0.375	0.219	–
r^2_{pred}	0.113	0.345	0.384	0.281	0.342	0.343	0.399	0.106
r^2_{bs}	0.624	0.997	0.996	0.957	0.968	0.991	0.989	0.986
Std dev	0.145	0.002	0.005	0.025	0.022	0.005	0.006	0.007

S = steric, E = electrostatic, D = H-bond donor, A = H-bond acceptor, and H = hydrophobic.

differences in electrostatic interactions with the FTase active site. Fig. 2 depicts CoMFA steric and electrostatic contour plots and Fig. 3 shows the graph of actual versus fitted/predicted activities for training and test set molecules.

2.1.2. 2-Amino-nicotinonitriles

2-Aminonicotinonitriles developed by Wang et al. [48] as farnesyltransferase inhibitors have been used to generate 3D-QSAR models initially from 44 compounds in training set (Table S2) and 15 in test set (Analysis A′). But this model displayed high standard error (0.463) and low r^2_{pred} (0.357) values. Hence, in order to improve the predictive power of the model, compounds whose residual values were higher were removed as outliers. A statistically significant model (using Analysis B′) was then obtained with cross-validated r^2 (r^2_{cv}) 0.803 with four components, low standard error of prediction (SEP) 0.285, non-cross-validated r^2 (r^2_{ncv}) 0.983 and predictive r^2 (r^2_{pred}) as high as 0.811. The respective steric and electrostatic field contributions were 54.2% and 45.8%. The 3D contour maps generated from the above CoMFA model are shown in Fig. 4 and a graph of actual versus fitted/predicted activities for training/test set molecules is depicted in Fig. 5.

Table 5
CoMFA versus CoMSIA

	I[a]		II[b]		III[c]	
	CoMFA	CoMSIA	CoMFA	CoMSIA	CoMFA	CoMSIA
r^2_{cv}	0.596	0.469	0.803	0.814	0.479	0.411
N_c	6	8	4	5	8	8
SEP	0.414	0.648	0.285	0.280	0.422	0.444
r^2_{ncv}	0.945	0.923	0.983	0.931	0.993	0.984
SEE	0.224	0.247	0.089	0.171	0.048	0.074
F-Value	62.660	41.883	261.653	101.184	373.34	158.62
$P\ r^2 = 0$	0.0	0.0	0.0	0.0	0.0	0.0
r^2_{pred}	0.790	0.787	0.811	0.784	0.686	0.399
r^2_{bs}	0.971	0.962	0.988	0.939	0.996	0.989
Std dev	0.013	0.023	0.004	0.019	0.003	0.006

[a] 3-Aminopyrrolidinone derivatives.
[b] 2-Amino-nicotinonitriles.
[c] 1-Aryl-1′-imidazolyl methyl ethers.

2.1.3. 1-Aryl-1′-imidazolyl methyl ethers

1-Aryl-1′-imidazolyl methyl ether derivatives [13] (Table S3) with selective FTase inhibitory activity developed by cancer research group at Abbott laboratories were used in the generation of 3D-QSAR models. Similar to above two structurally diverse classes of FTase inhibitors, initial CoMFA model (using Analysis A″) gave significantly poor statistical results with low cross-validated r^2 (r^2_{cv}) 0.346 at eleventh component, high standard error of prediction (SEP) 0.403, *F*-value erratically rose to 1112.47 and finally the predictive power of the model (r^2_{pred}) was 0.374. After removing outliers a CoMFA model was developed from a training set comprising of 30 molecules and validated by 5 test set molecules. A combination of steric and electrostatic fields yielded the CoMFA model having r^2_{cv} 0.479 with eight components, r^2_{ncv} 0.993, predictive r^2 0.686 and exhibited higher electrostatic field contribution (61.1%). The 3D steric and electrostatic contour maps are depicted in Fig. 6, and the graph of actual versus fitted/predicted activities for training/test set molecules is shown in Fig. 7.

2.2. COMSIA models

To investigate the significance of hydrophobic and H-bond fields on the FTase inhibitory activity, CoMSIA analysis using steric, electrostatic, hydrophobic and H-bond fields were carried out employing the same atom-based alignment used in CoMFA studies for all the three sets of farnesyltransferase inhibitors. In the results summarized for CoMSIA analysis, steric and electrostatic fields are not reported individually as the statistical results and position of contour maps did not vary significantly from that of CoMFA.

2.2.1. 3-Aminopyrrolidinone derivatives

The results of CoMSIA PLS analysis are summarized in Table 2. The CoMSIA model generated from steric and electrostatic fields did not vary both in terms of statistical values and positions of contours as compared to its CoMFA model and hence are not included in the table. Incorporation of the H-bond donor/acceptor or both fields yielded models with an improved external prediction, with predictive r^2 value of 0.665. These models showed comparable predictions, but the standard error was on a higher side and also the cross-validated r^2 was low (0.30). Hence they were considered to be of less statistical significance. Further hydrophobic fields were incorporated in order to study its influence on the model. A statistically significant and robust model was obtained. The combinations of steric, electrostatic, H-bond donor and acceptor fields and hydrophobic fields yielded CoMSIA models with an improved r^2_{cv} 0.469 with eight components, highest predictive value of r^2 0.787, r^2_{ncv} 0.923, r^2_{bs} 0.969 with steric (12.2%), electrostatic (21.1%), hydrophobic (12.7%), H-bond donor (23.4%) and acceptor (30.6%) field contributions. The 3D

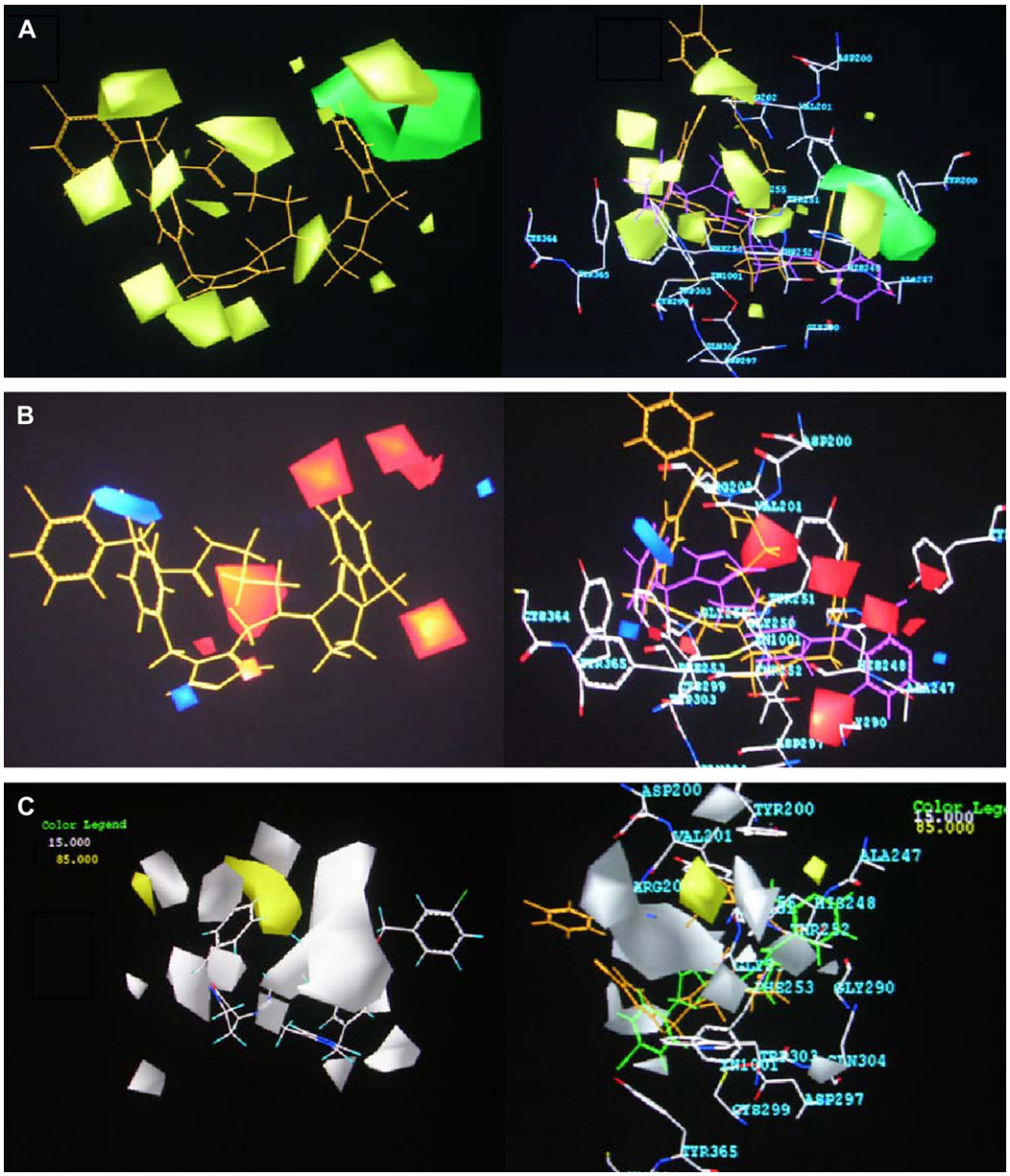

Fig. 2. STDDEV*COEFF contour plots for 3-aminopyrrolidinones. (A) CoMFA steric contours (green polyhedron: sterically favored; yellow polyhedron: sterically disfavored) and their superimposition on FTase active site. (B) CoMFA electrostatic (red polyhedron: negatively charged favored; blue polyhedron: positively charged favored) maps and their superimposition on FTase active site. (C) CoMSIA hydrophobic (yellow polyhedra: favored hydrophobic substituents; white polyhedra: disfavored hydrophobic substituents) contours and their superimposition on FTase active site. Compound **47** (orange) is the most active and compound **31** (least active) is shown in violet, purple and green in A, B, and C, respectively. (For interpretation of the references to colour in this figure legend, the reader is referred to the web version of this article.)

contours analyzed using this model is shown in Fig. 2. The graph of actual versus fitted/predicted activities for training/test set molecules is depicted in Fig. 3. The CoMSIA studies signify the contribution of H-bond donor, acceptor and hydrophobic fields in addition to steric and electrostatic fields towards the FTase inhibitory activity of 3-aminopyrrolidinones.

2.2.2. 2-Amino-nicotinonitriles

The results of PLS analysis for CoMSIA are summarized in Table 3. The PLS of CoMSIA analysis generated from steric, hydrophobic, H-bond donor and acceptor fields showed r^2_{cv} 0.705 with five components, the corresponding r^2_{ncv} as 0.968 and predictive r^2 0.757. The model generated using steric, electrostatic, hydrophobic and H-bond donor exhibited significant contribution of hydrophobic and electrostatic fields with improved statistical correlation coefficients r^2_{cv} 0.827, r^2_{ncv} 0.939 and predictive r^2 0.695. Further model obtained with the combination of steric, electrostatic, H-bond donor and hydrophobic fields showed r^2_{cv} 0.806, r^2_{ncv} 0.974 and predictive r^2 of 0.747. The model generated using all five CoMSIA fields yielded statistically significant model with r^2_{cv} 0.814 for five components, r^2_{ncv} 0.931, r^2_{bs} 0.949 and r^2_{pred} 0.784 and

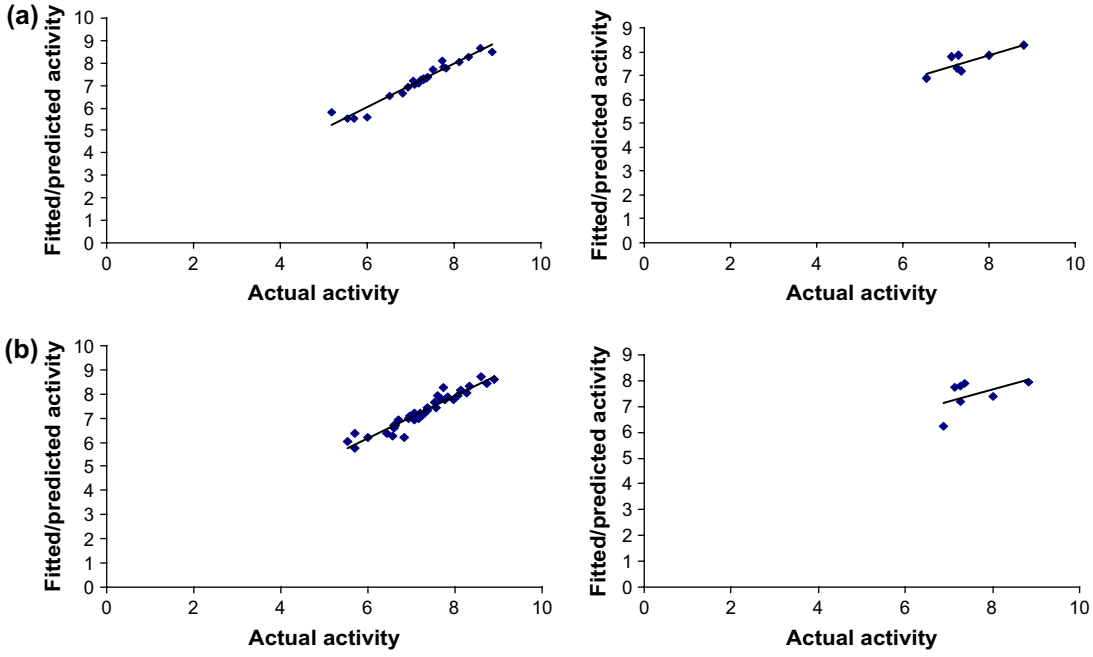

Fig. 3. A graph of actual versus fitted/predicted activities for training and test set molecules of 3-aminopyrrolidinones: (a) CoMFA; (b) CoMSIA.

respective field contributions was steric 8.5%, electrostatic 30.6%, hydrophobic 21.4%, H-bond donor 18.7% and acceptor 20.7%. This model with good internal and external predictions was used to analyze 3D contour plots (Fig. 4). The plot depicting actual versus fitted/predicted activities of data set molecules is shown in Fig. 5. The analysis of CoMSIA model showed higher contributions of hydrophobic and electrostatic fields to the FTase inhibitory activity of 2-amino-nicotinonitrile derivatives.

2.2.3. 1-Aryl-1′-imidazolyl methyl ethers

Table 4 summarizes the results of CoMSIA PLS analysis for 1-aryl-1′-imidazolyl methyl ethers. The model generated from the steric, electrostatic and H-bond donor fields exhibited better predictions with r^2_{cv} 0.451 at eight components, r^2_{ncv} 0.934, predictive r^2 0.342 and higher H-bond acceptor field (67.7%) contribution. The combination of steric, electrostatic and hydrophobic fields yielded poor external predictions with r^2_{pred} 0.280. The combination of steric, electrostatic, H-bond donor and acceptor fields yielded statistically significant model as compared to all other combinations and exhibited r^2_{cv} 0.444 with eight components, r^2_{ncv} 0.984, predictive r^2 0.400 with field contribution of steric 9.3%, electrostatic 26.6%, H-bond donor 0.8% and acceptor 21.9%. The 3D contours analyzed for generated model are shown in Fig. 6. The graph of actual versus fitted/predicted activities for training/test set molecules is depicted in Fig. 7. The models derived from other combinations like SDH, SEDH, HAD resulted in poor r^2_{pred} values and were considered to be of poor statistical significance. FTase inhibitory activity of 1-aryl-1′-imidazolyl methyl ethers was found to be contributed significantly by H-bond acceptor and electrostatic fields.

2.3. Graphical interpretation of the CoMFA and CoMSIA models

The steric contour maps indicate green and yellow contours as sterically favorable and unfavorable areas. Blue and red contours in the electrostatic maps indicate areas where positive and negative charge substituents favor activity. Hydrophobic, H-bond donor and acceptor contour maps indicate favorable yellow, cyan, magenta contours and disfavorable by white, violet/purple and red contours, respectively. Although the contour maps cannot be used as receptor maps, useful interpretations can be derived. The generated contour maps were mapped on the FTase active site, and fields were analyzed with respect to the amino acid residues of FTase. To aid in visualization, the template molecule in each class of compounds is displayed in the respective figures and the contour maps are discussed with the reference compound.

2.3.1. 3-Aminopyrrolidinones

Figs. 2(A) and 3(B) correspond to the CoMFA steric and electrostatic contour maps for 3-aminopyrrolidinones with the active molecule (compound **47**). The green contour observed in the vicinity of chlorine suggests that steric substituents in these regions may favor activity (compounds **22**, **24**, **35** and **47**), while the disfavored yellow contours in the vicinity of nitrogen attached to oxopyrrolidinone and *tert*-butoxycarbonylamino propyl group restrict steric substitution indicating decreased biological activity (compounds **37–41** and **1–12**). In the CoMFA electrostatic map, the red contour surrounding chlorine on ring 'X' indicates the significance of negatively charged/electron rich group for biological activity (compounds **47–51**). It was clearly observed that if 'X' ring is unsubstituted, the biological activity tends to decrease (compounds

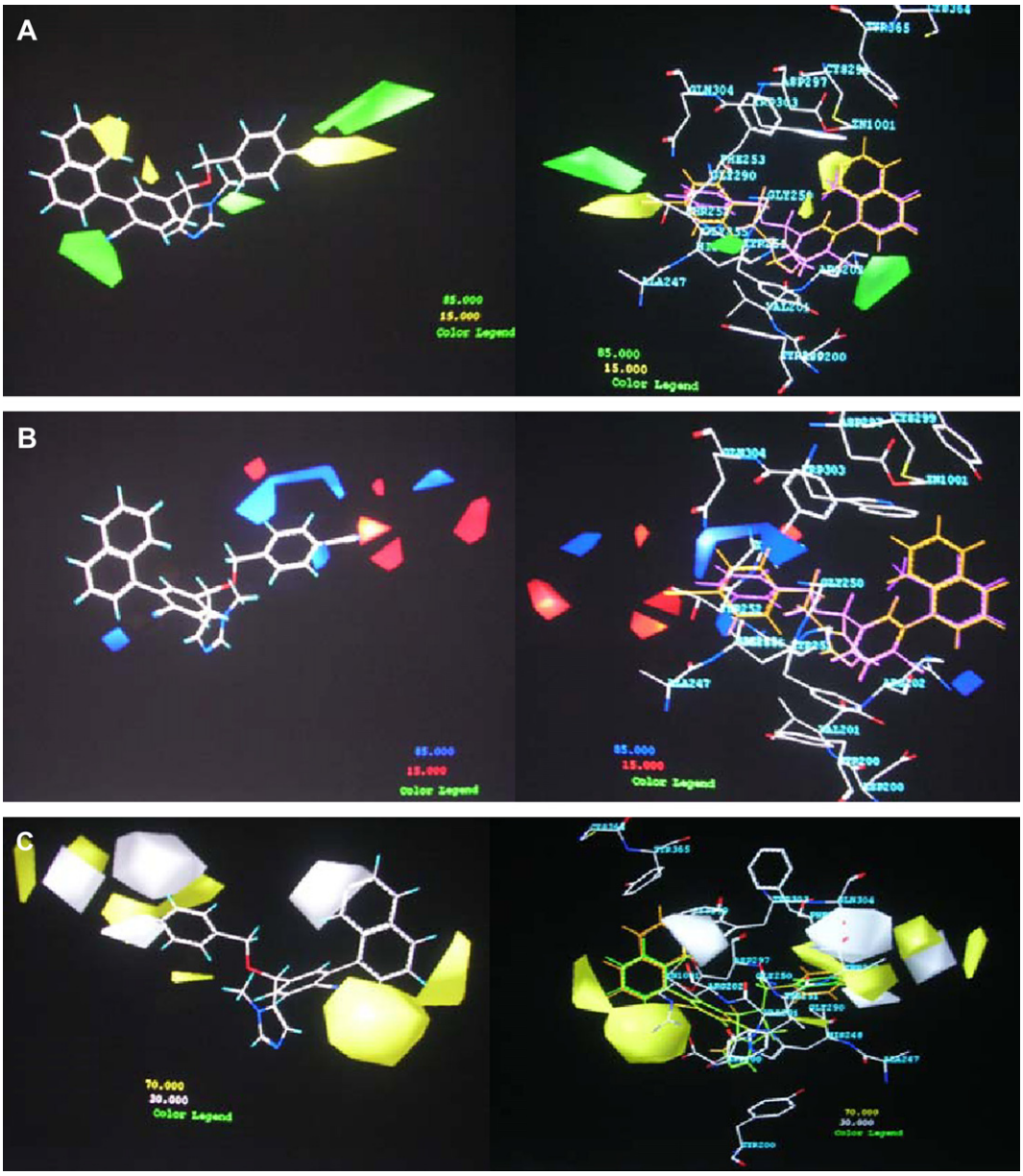

Fig. 4. STDDEV*COEFF contour plots for 2-aminonicotinonitriles. (A) CoMFA steric contours and their superimposition on FTase active site. (B) CoMFA electrostatic maps and their superimposition on FTase active site. (C) CoMSIA hydrophobic contours and their superimposition on FTase active site. Compound **97** (orange) is the most active and compound **51** (least active) is shown in violet, purple and green in A, B, and C, respectively. (For interpretation of the references to colour in this figure legend, the reader is referred to the web version of this article.)

38–**40**). The blue contour overlapping the cyano group of ring 'Y' indicates the significance of positively charged group for biological activity.

CoMFA steric and electrostatic contour plots mapped on FTase active site are depicted in Figs. 2(A) and 3(B) with highest active compound **47** (orange) and lowest active compound **31** (violet). The sterically favored green contour was placed in between His 248 and Tyr251, while disfavored yellow contours were observed at the periphery of Tyr365, Arg202 and overlapping phenyl ring of Phe253. The orientation of oxopyridinone ring towards zinc may be one of the major reasons why compound **47** is more active as the possibility of oxopyridinone ring oxygen forming bond with zinc is more, which is not the case with the least active compound **31**. The positively charged favored blue contour near the cyano substituent on ring 'Y' was placed close to Arg202 and Trp303, while small negatively charged red contour was observed near Val201, Asp297 and His248. 4-Cl may have van der Waals contact with Try 251.

Fig. 2(C) displays the CoMSIA hydrophobic contour maps and their overlapping on the FTase active site with compound **47**. The hydrophobic contour plots connotate disfavored large white regions in the vicinity of rings 'X' and 'Y', which are found overlapping on Arg202. Also small disfavored white contours are seen overlapping the *tert*-butoxycarbonylamino substituent near to Thr252 and Phe253, which indicate that

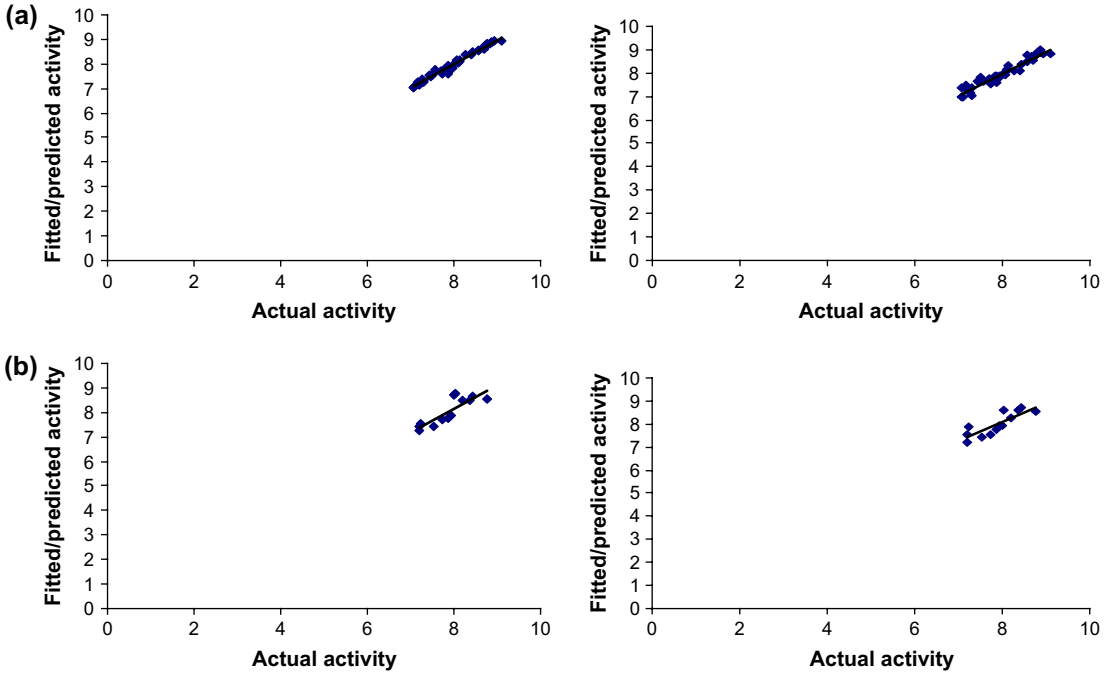

Fig. 5. A graph of actual versus fitted/predicted activities for training and test set molecules of 2-amino-nicotinonitriles: (a) CoMFA; (b) CoMSIA.

optimum lipophilic substituents may decrease or enhance the biological activity. Favored yellow region in the vicinity of benzyl group indicate the significance of lipophilic substituents for biological activity. The CoMSIA steric and electrostatic contour maps appear in the same region as that of CoMFA and hence are not discussed here.

CoMSIA H-bond donor contour maps are displayed in Fig. S4(A). H-bond donor favoring cyan contour was observed near −NH of *tert*-butoxycarbonylamino substituent of compound **47**, indicating that H-bond donor groups in this region may favor activity (compounds **48**–**50**). Further, compounds which lack H-bond donor substituents in these regions showed decreased activity (compounds **1**–**12**). Unfavorable purple contours were observed close to benzyl attached to oxopyridinone and on the planar surface near the carbonyl amide linkage of compound **47**. H-bond acceptor contour maps (Fig. S5) show favorable magenta contours in the vicinity of carbonyl and cyano group of compound **47** indicating its significance for biological activity.

2.3.2. 2-Amino-nicotinonitriles

The CoMFA steric and electrostatic contour plots with the template molecule (compound **97**) and its superimposition on FTase active site are shown in Fig. 5(A) and 5(B). The CoMFA steric plot portraying sterically favoring green polyhedra near to napthyl ring suggests that optimum steric substituents in this region favor activity (compounds **103**–**111**). A small green contour in the vicinity of ring 'A' indicates its significance for biological activity, whereas sterically disfavored yellow contours were observed in the vicinity of −CN group indicating restriction for incorporating steric substituents which may decrease FTase inhibitory activity (compounds **51**, **55**, **56**). CoMFA electrostatic contour plots displayed a positively charged favored large blue contour surrounding ring 'A' which signifies that an increase in activity may be due to low electron density substituents, while small negatively charged favored red contours near 4-CN (ring A) specify that the electron rich substituents favor activity (compounds **61**, **63**, **98**–**102**). Moderate activity was observed for compounds **64** and **76**.

Fig. 5(A) and 5(B) portrays mapping of CoMFA steric and electrostatic contour maps on the active site of farnesyltransferase. The sterically favored green contour is seen placed at the periphery of Arg202 and also close to Gly255 and Tyr251, while disfavored yellow contours were seen close to zinc and Thr252. The positively charged favored blue contour surrounding ring 'A' was observed overlapping over Gly290. The small negatively charged red contour on the upper part of 4-CN on ring 'A' was observed near Thr252 where 4-CN might have van der Waals contact.

The CoMSIA steric and electrostatic contour maps and its mapping on FTase active site are displayed in Fig. S6(A) and (B), respectively, with compound **97**. In the steric contour map a large favorable green contour was observed near ring 'A', suggesting that optimum steric substituents in this region favor activity (compounds **61**, **76**, **103**–**111**). These contours are seen overlapping Gln304 and close to Trp303. Sterically unfavorable yellow contour placed near to Tyr365 was observed close to the methyl substituent on the five-membered ring indicating restricted area for bulkier substituents. This may be one of the reasons for poor biological activity of compound **31** (shown in purple). CoMSIA electrostatic contour maps are not discussed as they were placed in regions similar to that observed in CoMFA.

Fig. 4(C) displays the CoMSIA hydrophobic contour map and its superimposition on the FTase active site with highest

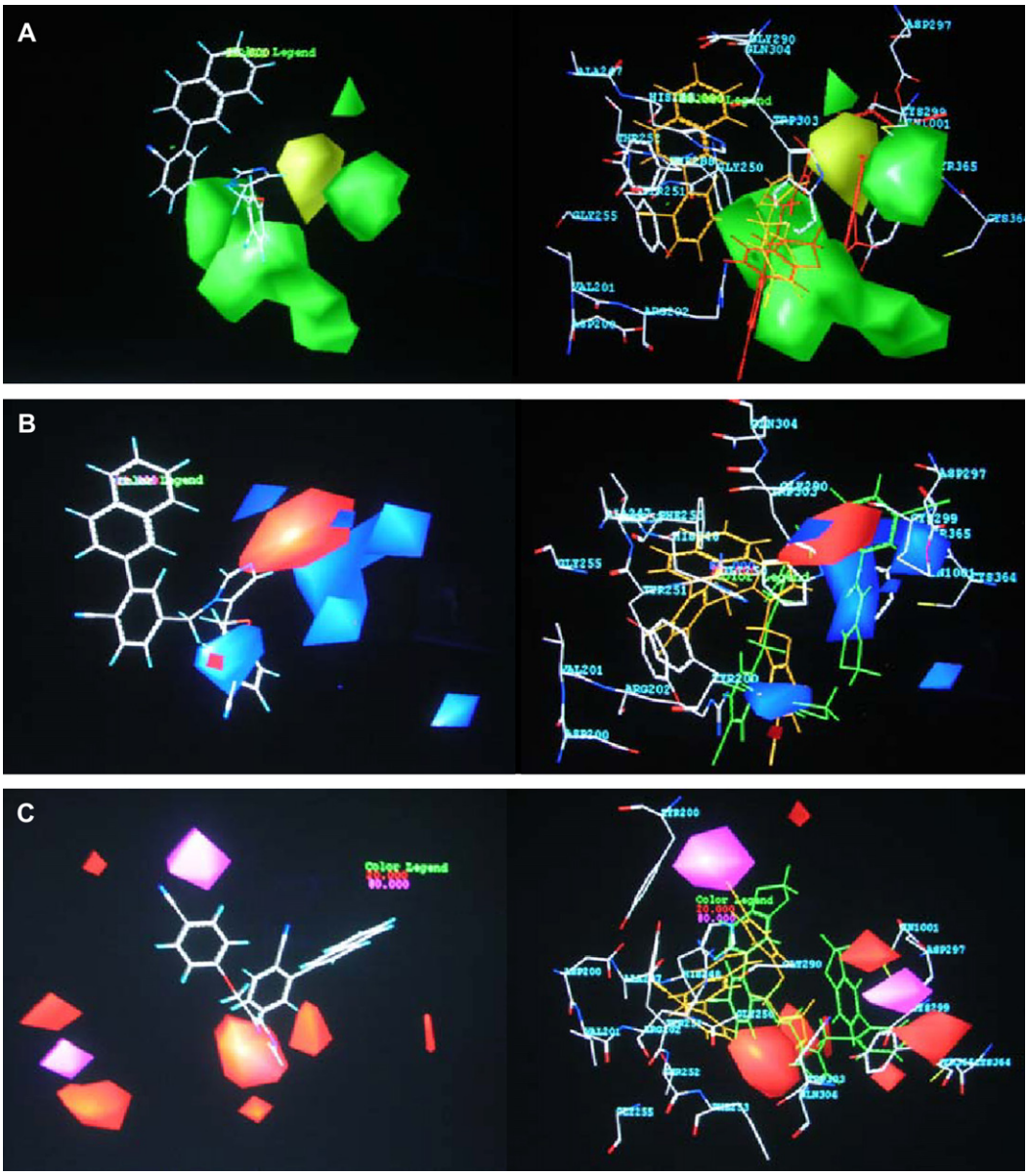

Fig. 6. STDDEV*COEFF contour plots for 1-aryl-1′-imidazolyl methyl ethers. (A) CoMFA steric contours and their superimposition on FTase active site. (B) CoMFA electrostatic maps and their superimposition on FTase active site. (C) CoMSIA H-bond acceptor contours and their superimposition on FTase active site. Compound **152** (orange) is the most active and compound **145** (least active) is shown in red, green and green in A, B, and C, respectively. (For interpretation of the references to colour in this figure legend, the reader is referred to the web version of this article.)

active compound **97**. In the hydrophobic contour map, favorable yellow contours were observed in the vicinity of cyano group of rings 'A', 'B' and napthyl ring where increased lipophilic substituents may favor activity (compounds **98**–**102**), while disfavored white contours were seen in the vicinity of napthyl ring and ring 'A' indicating regions where hydrophilic substituents may enhance activity and lipophilic substituents may decrease activity (compounds **85**–**87**). The hydrophobic contour plots which connotate disfavored white regions close to napthyl ring and ring 'A' occupy space between Zinc–Cys299 and Gln304–Thr302, respectively, while favored yellow contours are seen in the periphery of Asp300 and surrounding Thr252.

Fig. S7 displays CoMSIA H-bond donor contour maps. The CoMSIA H-bond donor contour map depicts large favorable cyan contours adjacent to ring 'A' and parallel to ring 'B' in the vicinity of napthyl ring signifying the presence of H-bond donor groups in these regions for FTase inhibitory activity (compounds **91**, **95**, **101**, **102**). This can be considered as one of the reasons why Wang and his co-researchers [48] considered cyano group as an optimum *para*-substituent on both rings 'A' and 'B' throughout the series of compounds synthesized for FTase inhibitory activity.

2.3.3. 1-Aryl-1′-imidazolyl methyl ethers

Figs. 6(A) and 7(B) correspond to the CoMFA steric and electrostatic contour maps and its mapping on FTase active site for 1-aryl-1′-imidazolyl methyl ethers with the active molecule (compound **152**). The large green contour observed in

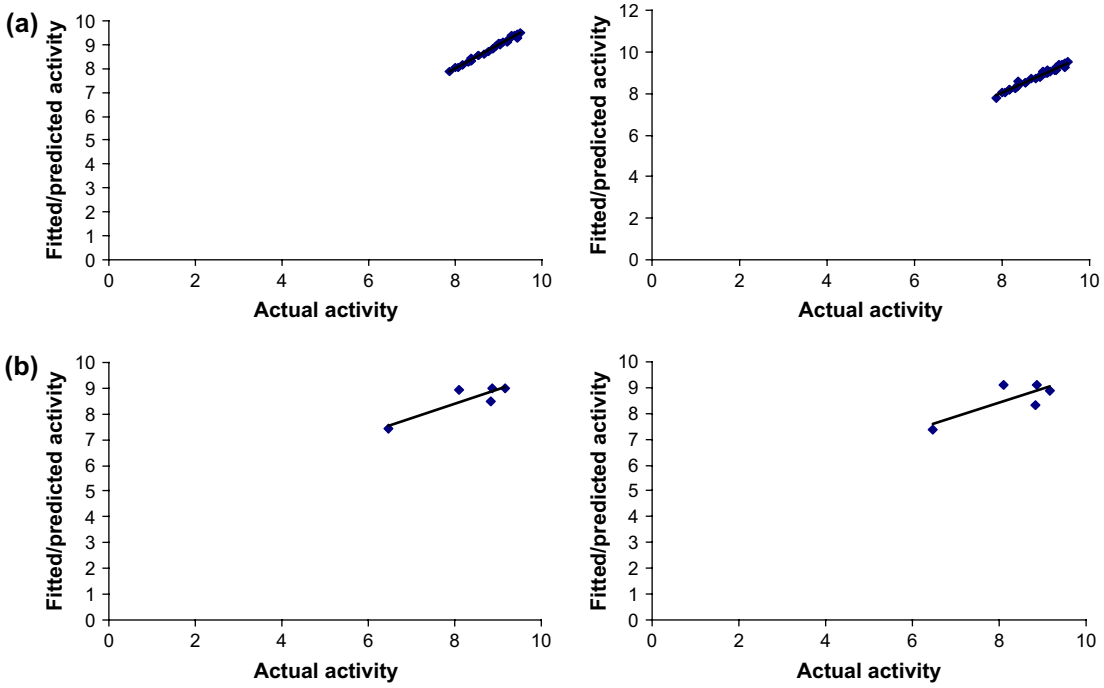

Fig. 7. A graph of actual versus fitted/predicted activities for training and test set molecules of 1-aryl-1′-imidazolyl methyl ethers: (a) CoMFA; (b) CoMSIA.

the vicinity of ring 'C' suggests that steric substituents in this region may favor activity (compounds **141**–**143**, **151**). The green contour was observed near to Arg202 and one more sterically favorable small green contour occupied space between Cys364 and Cys299 overlapping Try302. The disfavored yellow contour surrounding the imidazole ring restricts steric substitution indicating decreased biological activity. It was found placed close to zinc and Trp303. In the CoMFA electrostatic map, blue contour embedded in ring 'C' indicates the significance of positively charged group for farnesyltransferase inhibitory activity (compounds **127**, **130**, **131**) which was observed in the periphery of Cys299, Tyr365 and zinc, while small negatively charged favored red contour near imidazole nucleus specify that electron rich substituents favor activity.

In this class of compounds, the CoMSIA steric and electrostatic contour maps were not of much significance as they appeared at almost the same positions as those observed in CoMFA and hence not discussed. Not much significant difference in the position of CoMSIA steric and electrostatic contour maps was observed as compared to CoMFA, but these steric and electrostatic contour maps and their superimposition on FTase active site is depicted in Fig. S8(A) and (B) (see Supporting information).

CoMSIA H-bond acceptor contours and their overlapping on FTase active site are displayed in Fig. 6(C) with compound **152**. The H-bond acceptor contour maps show favorable magenta contours in the vicinity of *para*-cyano group of ring 'C' near to Tyr200 signifying the presence of H-bond donor groups for biological activity (compounds **117**, **150**), while small disfavorable red contours embedded in imidazole ring and in the vicinity of *ortho*-substitution on ring 'D' restricts substitution of H-bond donor groups which may decrease the biological activity. The disfavorable red contours occupied space in the vicinity of Gly250, Trp303 and Gln304. It can be observed that *p*-cyano group of ring 'C' orients towards favored magenta contour in case of compound **152** with potent inhibitory activity, while this is not the case with **145** (shown in green) as it has orientation which does not favor FTase inhibitory activity.

3. Experimental

3.1. Biological data

The training and test sets used in the computational studies comprise of molecules belonging to different chemical classes as reported as FTase inhibitors. The FTase inhibitory data has been collected from the literature [47–49]. The in vitro inhibitory activity IC_{50} (nM) against FTase converted to pIC_{50} (nM, $pIC_{50} = \log 1/IC_{50}$) was used as dependent variable in deriving 3D-QSAR models. The structures and biological activity data of training and test set molecules are described in Tables S1–S3 (see Supporting information). The X-ray crystallographic structures of FTase were taken from the Protein Data Bank (pdb codes – 1NL1 and 1NL4).

3.2. Molecular modeling

All computational studies were performed using Sybyl 7.0 [50] software running on Silicon Graphics Fuel workstation. The 3D structures of molecules were built using the 'Sketch Molecule' function within Sybyl. Initial optimization of the structures was carried out using TRIPOS force field with MMFF94 charges and repeated minimization was performed

using steepest descent and conjugated gradient methods till the root-mean-square (rms) deviation of 0.001 kcal/mol was achieved. Conformational energies were calculated with electrostatic terms; the lowest energy structures finally minimized were used in superimpositions. The partial atomic charges required for the electrostatic interaction were computed by a semi empirical molecular orbital method using MOPAC [51] with AM1 Hamiltonian [52]. Development of predictive 3D-QSAR CoMFA models is essentially alignment sensitive that defines the putative pharmacophore for the series of ligands under investigation. Atom-based alignment approach has been employed in order to calculate the CoMFA and CoMSIA interaction energies (Fig. 1).

3.3. CoMFA and CoMSIA analyses

3.3.1. CoMFA analysis

All of the CoMFA experiments were performed on Silicon Graphics Fuel workstation with the molecular modeling software *Sybyl 7.0*. The molecular atomic charges were calculated using the Gasteiger–Huckel protocol. The steric and electrostatic field energies were calculated using field's viz. standard CoMFA field, H-bonding fields, indicator fields and parabolic fields [53,54] for the CoMFA calculation. All the models were investigated using the full cross-validated partial least-squares (PLS) (leave-one-out) method with CoMFA standard options for the scaling of variables. Column filtering was set to 2.0 kcal/mol to improve the signal-to-noise ratio by omitting those lattice points whose energy variation is below this threshold. The statistical significance and predictive ability of the resulting models were assessed using leave-one-out cross-validated r^2, also called as q^2. The conventional r^2 was considered as a measure of the predictive ability within the training set, while the q^2 has been considered as a measure of predictive ability outside the training set.

3.3.2. CoMSIA analysis

The CoMSIA technique exhibits greater robustness with respect to both region shifts and small shifts within the alignments with no application of arbitrary cutoffs and more intuitively interpretable contour maps. The standard setting (probe with charge +1, radius 1 Å and hydrophobicity +1, hydrogen bond donating +1, hydrogen bond accepting +1, attenuation factor a of 0.3 and grid spacing 2 Å) was used in CoMSIA to calculate seven different fields viz. steric, electrostatic, hydrophobic, hydrogen bond donor, hydrogen bond acceptor, steric and electrostatic, and hydrogen bond donor and acceptor.

3.3.3. Partial Least Square (PLS) analysis

The CoMFA/CoMSIA descriptors served as independent variables and pIC_{50} (nM) values as dependent variables in PLS regression analysis for deducing 3D-QSAR models [55]. Normally cross-validation is used to check the predictive power of the derived model. The result of analysis corresponds to the regression equation with thousands of coefficients. The predictive values of models were evaluated using leave-one-out (LOO) cross-validation method. The number of components leading to the highest cross-validated r^2 and lowest standard error of prediction (SEP) was set as the optimum number of components (N_c) in PLS analysis. σ Minimum of 2.0 kcal/mol was used as the threshold column filtering value in PLS analysis. To obtain the statistical confidence limit in the analyses, PLS analysis using 100 bootstrap groups with an optimum number of components was performed.

3.3.4. Predictive ability of CoMFA and CoMSIA models

The predictive ability of each analysis was determined from test set molecules that were not included in the training set. These molecules were aligned, and there activities were predicted by each PLS analysis. The predictive r^2 (r^2_{pred}) value defined as

$$r^2_{pred} = (SD - PRESS)/SD$$

where, SD is the sum of squared deviations between the biological activities of the test set and mean activity of the training set molecules, and PRESS is the sum of squared deviation between actual and predicted activities of the test set molecules.

4. Conclusion

3D-QSAR studies yielded stable and statistically significant predictive models indicated by the moderate to high cross correlation coefficients. A high bootstrapped r^2 value and a small standard deviation indicate that a similar relationship exists in all the compounds of the series used in the study. All the CoMFA models generated using the atom-based rms fitting method exhibited statistically significant and predictive models after the removal of outliers. The steric and electrostatic field contributions revealed relatively higher contributions of electrostatic fields except for 2-amino-nicotinonitrile class that showed higher contributions of steric fields.

The comparison of CoMFA and CoMSIA models obtained using steric and electrostatic fields suggests that CoMFA yielded relatively improved models for 3-aminopyrrolidinones and 1-aryl-1′-imidazolyl methyl ethers. CoMSIA yielded fairly improved models for 2-amino-nicotinonitriles and statistically insignificant models for 1-aryl-1′-imidazolyl methyl ethers. Overall CoMFA yielded comparable models for 3-aminopyrrolidinones and 1-aryl-1′-imidazolyl methyl ethers highlighting the significance of steric and electrostatic fields towards FTase inhibitory activity. While CoMSIA models were statistically significant for 2-amino-nicotinonitriles indicating the importance of hydrophobic, H-bond donor and acceptor fields towards FTase inhibitory activity. The CoMSIA steric and electrostatic field maps are in accordance with field distribution of CoMFA maps and consistent with structure–activity relationships. The comparison of 3D-QSAR models with the active site of FTase revealed the interactions of amino acid residues with the substructures of molecules with steric, electrostatic, hydrophobic and H-bond donor and acceptor fields.

In the present study, we have identified the significance of various structural elements binding to active site which may be

combined to improve the overall activity. Overall, the present 3D-QSAR study investigates the indispensable structural features of the different chemical classes of molecules which can be exploited for the structural modifications of these lead molecules in order to achieve improved selective FTase inhibitory activity.

Acknowledgements

We thank All India Council for Technical Education (A.I.C.T.E), New Delhi, India for financial support [File No. 8021/RID/NPROJ/TAP-201/2002-03]. D.S.P. is thankful to University Grants Commission, New Delhi, India for the award of Junior Research Fellowship [F.10-1/2004(SA-I)].

Appendix. Supporting information

Tables of structures and farnesyltransferase inhibitory activities of data sets (Tables S1–S3), CoMSIA (STDDEV*COEFF) H-bond donor contour plot and its superimposition on FTase active site and H-bond acceptor contour plot for 3-aminopyrrolidinones (Figs. S4(A), (B) and S5), CoMFA steric and electrostatic STDDEV*COEFF contour maps for 2-amino-nicotinonitrile class of compounds and its superimposition on FTase active site (Fig. S6(A) and (B)), CoMSIA H-bond donor contours for 2-amino-nicotinonitrile class of compounds (Fig. S7), CoMFA steric and electrostatic contour maps and their superimposition on FTase active site for 1-aryl-1′-imidazolyl methyl ether derivatives (Fig. S8(A) and (B)). Supplementary data associated with this article can be found in the online version, at doi:10.1016/j.ejmech.2007.02.003.

References

[1] A. Levitzki, A. Gazit, Science 267 (1995) 1782–1788.
[2] J.B. Gibbs, A. Oliff, Cell 79 (1994) 193–198.
[3] J.L. Bos, Cancer. Res. 49 (1989) 4862–4869.
[4] J.B. Gibbs, Cell 65 (1991) 1–4.
[5] A. Oliff, Biochim. Biophys. Acta 1423 (1999) C19–C30.
[6] B.M. Willumsen, K. Norris, A.G. Papageorge, N.L. Hubbert, D.R. Lowy, EMBO J. 3 (1984) 2581–2585.
[7] P.J. Casey, P.A. Solski, C. Der, J.E. Buss, Proc. Natl. Acad. Sci. U.S.A. 86 (1989) 8323–8327.
[8] W.J. Chen, J.L. Goldstein, M.S. Brown, Proc. Natl. Acad. Sci. U.S.A. 88 (1991) 11368–11372.
[9] W.J. Chen, D.A. Res, J.L. Goldstein, D.W. Russell, M.S. Brown, Cell 66 (1991) 327–334.
[10] P. Dunten, U. Kammlot, R. Crowther, D. Weber, R. Palermo, J. Birktoft, Biochemistry 37 (1998) 7907–7912.
[11] J.L. Goldstein, M.S. Brown, S.J. Stradley, Y. Reiss, L.M. Gierasch, J. Biol. Chem. 266 (1991) 15575–15578.
[12] J.B. Gibbs, D.L. Pompliano, S.D. Mosser, R.B. Lingham, S.B. Singh, E.M. Scolnik, N.E. Kohl, A. Oliff, J. Biol. Chem. 268 (1993) 7617–7620.
[13] D.M. Leonard, J. Med. Chem. 40 (1997) 2917–2990.
[14] S. Halazy, J.P. Gottel, M. Lamothe, D. Perrin, B.T. Hill, Drugs Future 20 (1997) 1133–1146.
[15] C.A. Omer, N.E. Kohl, Trends Pharmacol. Sci. 18 (1997) 437–445.
[16] Y. Qian, S.M. Sebti, A.D. Hamilton, Biopolymers 43 (1997) 25–41.
[17] S.M. Sebti, A.D. Hamilton, Drug Discov. Today 3 (1998) 26–32.
[18] C.L. Strickl, W.T. Windsor, R. Syto, L. Wang, R. Bond, R. Wu, J. Schwartz, H.V. Le, L.S. Beese, P.C. Weber, Biochemistry 37 (1998) 16601–16611.
[19] J.E.F. Reynolds (Ed.), Martindale: The Extra Pharmacopoeia, 31st ed. Royal Pharmaceutical Society of Great Britain, London, 1996, p. 821.
[20] J.T. Hunt, V.G. Lee, K. Leftheris, B. Seizenger, J. Carboni, J. Mabus, C. Ricca, N. Yan, V. Manne, J. Med. Chem. 39 (1996) 353–358.
[21] S.J. O'Connor, K.J. Barr, L. Wang, B.K. Sorenson, A.S. Tasker, H. Sham, A.C. Ng, J. Cohen, E. Devine, S. Cherian, B. Saeed, H. Zhang, J.Y. Lee, R. Warner, S. Tahir, P. Kovar, P. Ewing, J. Alder, M. Mitten, J. Leal, K. Marsh, J. Bauch, D.J. Hoffman, S.M. Sebti, S.H. Rosenberg, J. Med. Chem. 42 (1999) 3701–3710.
[22] D.J. Augeri, D. Janowick, D. Kalvin, G. Sullivan, J. Larsen, D. Dickman, H. Ding, J. Cohen, J. Lee, R. Warner, P. Kovar, S. Cherian, B. Saeed, H. Zhang, S. Tahir, A.C. Ng, H. Sham, S.H. Rosenberg, Bioorg. Med. Chem. Lett. 9 (1999) 1069–1074.
[23] M.J. Breslin, J. deSolms, E.A. Giuliani, G.E. Stokker, S.L. Graham, D.L. Pompliano, S.D. Mosser, K.A. Hamilton, J.H. Hutchinson, Bioorg. Med. Chem. Lett. 8 (1998) 3311–3316.
[24] T.M. Ciccarone, S.C. MacTough, T.M. Williams, C.J. Dinsmore, T.J. O'Neill, D. Shah, J.C. Culberson, K.S. Koblan, N.E. Kohl, J.B. Gibbs, A.I. Oliff, S.L. Graham, G.D. Hartman, Bioorg. Med. Chem. Lett. 9 (1999) 1991–1996.
[25] A.M. Garcia, C. Rowell, K. Ackermann, J.J. Kowalczyk, M.D. Lewis, J. Biol. Chem. 268 (1993) 18415–18418.
[26] J.B. Gibbs, A. Oliff, N.E. Kohl, Cell 77 (1994) 175–178.
[27] M. Crul, G.J. de Klerk, J.H. Beijnen, J.H. Schellens, Anti-Cancer Drugs 12 (2001) 163–184.
[28] S.B. Singh, R.B. Lingham, Curr. Opin. Drug Discov. Dev. 5 (2002) 225–244.
[29] R. Doll, IDrugs 4 (2001) 1382–1388.
[30] K. Zhu, A.D. Hamilton, S.M. Sebti, Curr. Opin. Invest. Drugs 4 (2003) 1428–1435.
[31] F. Caponigro, M. Casale, J. Bryce, Expert. Opin. Invest. Drugs 12 (2003) 943–954.
[32] I.M. Bell, J. Med. Chem. 47 (2003) 1869–1878.
[33] C.Y. Huang, L. Rokoz, Exp. Opin. Ther. Pat. 14 (2004) 175–186.
[34] A.G. Taveras, P.K. Kirschmeier, C.M. Baun, Curr. Top. Med. Chem. 10 (2003) 1103–1114.
[35] G.L. James, J.L. Goldstein, M.S. Brown, T.E. Rawson, T.C. Somers, Science 260 (1993) 1937–1942.
[36] W.R. Bishop, R. Bond, J. Petrin, L. Wang, R. Doll, J. Biol. Chem. 270 (1995) 30611–30618.
[37] R.D. Crammer III, D.E. Patterson, J.D. Bunce, J. Am. Chem. Soc. 110 (1998) 5959–5967.
[38] T.T. Talale, S.S. Kulkarni, V.M. Kulkarni, J. Chem. Inf. Comput. Sci. 39 (1999) 958–966.
[39] S.V. Murthy, V.M. Kulkarni, Bioorg. Med. Chem. 10 (2002) 2267–2282.
[40] H. Gohlke, G. Klebe, J. Med. Chem. 45 (2002) 4153–4170.
[41] R.D. Crammer III, J. Med. Chem. 46 (2003) 374–388.
[42] G. Klebe, U. Abraham, T. Mietzner, J. Med. Chem. 37 (1994) 4130–4146.
[43] M. Bohm, J. Sturzebecher, G. Klebe, J. Med. Chem. 42 (1999) 458–477.
[44] G. Klebe, Perspect. Drug Discov. Des. 12 (1998) 87–104.
[45] D.S. Puntambekar, R. Giridhar, M.R. Yadav, Bioorg. Med. Chem. Lett. 16 (2006) 1821–1827.
[46] D.S. Puntambekar, R. Giridhar, M.R. Yadav, Eur. J. Med. Chem. 41 (2006) 1279–1292.
[47] I.M. Bell, S.N. Gallicchio, M. Abrams, D.C. Beshore, C.A. Buser, J.C. Culberson, J. Davide, M. Ellis-Hutchings, C. Fernes, J.B. Gibbs, S.L. Graham, G.D. Hartman, D.C. Heimbrook, C.F. Homnick, J.R. Huff, K. Kassahun, K.S. Koblan, N.C. Kohl, R.B. Lobell, J.J. Lynch, P.A. Miller, C.A. Omer, A.D. Rodrigues, E.S. Walsh, T.M. Williams, J. Med. Chem. 44 (2001) 2933–2949.
[48] Q. Li, G.T. Wang, T. Li, S.L. Gwaltney, K.W. Woods, A. Claiborne, X. Wang, W. Gu, J. Cohen, V.S. Stoll, C. Hutchins, D. Frost, S.H. Rosenberg, H.L. Sham, Bioorg. Med. Chem. Lett. 14 (2004) 5371–5376.

[49] G.T. Wang, X. Wang, W. Wang, L.A. Hasvold, G. Sullivan, C.W. Hutchins, S. O'Conner, R. Gentiles, T. Sowin, J. Cohen, W.Z. Gu, H. Zhang, S.H. Rosenberg, H.L. Sham, Bioorg. Med. Chem. Lett. 15 (2005) 153–158.
[50] The program Sybyl 7.0 is available from Tripos Inc., 1699, South Hanley Road, St. Louis, MO 63144, U.S.A.
[51] J.J. Stewart, J. Comput.-Aided Mol. Des. 4 (1990) 1–105.
[52] M.J.S. Dewar, E.G. Zoebisch, E.F. Healy, J.P.P. Stewart, J. Am. Chem. Soc. 107 (1985) 3902–3909.
[53] R.S. Bohacek, C. McMartin, J. Med. Chem. 35 (1992) 1671–1684.
[54] R.T. Kroemer, P. Hecht, J. Comput.-Aided. Mol. Des. 9 (1995) 205–212.
[55] (a) S. Wold, C. Albano, W.J. Dunn, U. Edlund, K. Esbenson, P. Geladi, S. Hellberg, E. Johansson, W. Lindberg, M. Sjostrom, Multivariate Data Analysis in Chemistry, in: B.R. Kowalski (Ed.), Chemometrics: Mathematics and Statistics in Chemistry, D. Reidel, Dordrecht, 1984, p. 17;
(b) S. Wold, A. Rune, H. Wold, W.J. Dunn, SIAM J. Sci. Stat. Comput. 5 (1984) 735–743;
(c) M. Clark, R.D. Crammer III, Quant. Struct.-Act. Relat. 12 (1993) 137–145;
(d) I.N. Wakeling, J.J. Morris, J. Chemom. 7 (1993) 291–304;
(e) S. Wold, in: H. van de Waterbeemd (Ed.), Chemometrics Methods in Molecular Design, VCH, New York, 1995, p. 195.